ACS Partner Journal

CHEMICAL & BIOMEDICAL IMAGING

pubs.acs.org/ChemBioImaging

Letter

Methylene Blue: An FDA-Approved NIR-II Fluorogenic Probe with Extremely Low pH Responsibility for Hyperchlorhydria Imaging

Guanjun Deng,[#] Siwei Zhang,[#] Xinghua Peng, Gongcheng Ma, Luxuan Liu, Yuyu Tan, Ping Gong,* Ben Zhong Tang,* Lintao Cai,* and Pengfei Zhang*

Cite This: *Chem. Biomed. Imaging* 2024, 2, 683−688

Read Online

ACCESS | Metrics & More | Article Recommendations | Supporting Information

ABSTRACT: Methylene blue (MB) is an FDA (Food and Drug Administration)-approved contrast agent with donor−acceptor (D−A) structure integrated with carbonyl-containing nitrogen-heterocycles. MB can be converted into MBH (protonated MB) by protonation, which not only induces the fluorescence emission red-shifted from the first near-infrared window (NIR-I, 650−950 nm) to the second near-infrared window (NIR-II, 1000−1700 nm) but also achieves ACQ-to-AIE conversion. MB has been successfully demonstrated in hyperacidemia imaging with an extremely low pH value (<1).

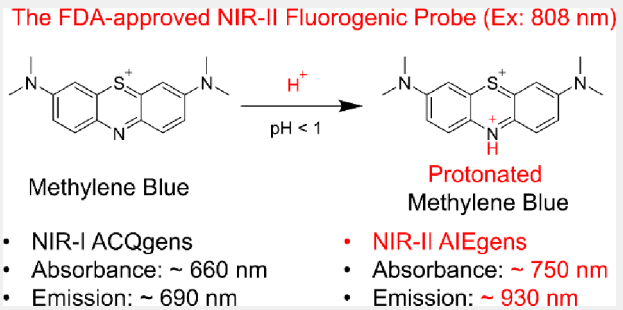

KEYWORDS: *aggregation-induced emission, NIR-II fluorescence, gastric hyperacidity, pH detection, FDA-approved*

Various luminescent materials such as organic and inorganic substances have gradually been studied.[1,2] Because they had an adjustable molecular structure and chemical composition, were easy to functionalize and synthesize, and had the potential to meet the expectations of biomedical related research, organic light-emitting materials had attracted more attention. The luminescent materials with emission ability in a wide wavelength range, such as ultraviolet light to near-infrared light, were also gradually discovered.[3−5] Unfortunately, when light-emitting molecules were used in their high concentration or aggregate state, aggregation-induced quenching (ACQ) often occurred, which limited their application.[6] Therefore, how to solve the ACQ problem has become one of the hottest studies in recent years. Most traditional luminophores emitted strong light when they existed in a single-molecule state, but when they existed in an aggregate state, the light emission was almost negligible. The traditional luminophores had a strong intermolecular $\pi-\pi$ interaction, leading to the aggregation-caused quenching (ACQ) effect.[7−9] Since 2001, luminescent materials with aggregation-induced emission properties (AIEgens) had received widespread attention.[10,11] However, the molecular design concept of the new AIEgens was still lacking, in contrast to the excellent optical properties and abundant ACQ molecules. So, the conversion of ACQ to AIE provided another way to design AIEgens, where twisted AIEgen, propeller molecules, or bulky substituents were incorporated into planar ACQ molecules to prevent compact interface accumulation.[12−15] However, these strategies were not applicable to all ACQ−AIE conversion systems; therefore, it was necessary to develop a new method to realize the ACQ−AIE conversion system.

Fluorescence imaging provided a powerful visualization tool to image dynamic and complex processes in living cells and animals.[16−18] The fluorophores with NIR-II emissions (1000−1700 nm) explicitly showed some advantages, such as higher spatiotemporal resolution in deep tissue and better signal-to-background ratio (SBR) compared with NIR-I fluorescence imaging (650−950 nm).[19−21] Some NIR-II probe systems were always in "on" mode, which could lead to low detection sensitivity and specificity, due to nonspecific background signals from healthy tissue and off-target.[22−24] However, theactivatable NIR-II fluorescence probe had superior potential characters to improved detection quality.[25,26] Recent experiments with an activatable NIR-II probe (FEAD1) that responded to the tumor microenvironment greatly improved the accuracy of tumor diagnosis, and its maximum SBR reached the level of 7.[27] Therefore, the development of an intelligent activatable NIR-II fluorescence probe was very important to improve detection sensitivity and specificity.

The pH value was a key parameter of great significance, which controlled many chemical or physiological processes.[28,29] Especially in biological systems, pH homeostasis

Received: January 31, 2024
Revised: April 7, 2024
Accepted: April 8, 2024
Published: April 12, 2024

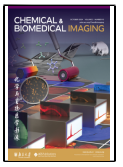

https://doi.org/10.1021/cbmi.4c00011
Chem. Biomed. Imaging 2024, 2, 683−688

was the prerequisite for the viability of living cells.[30] The pH changed from alkaline to highly acidic in various prokaryotes as well as different subcellular organelles of eukaryotic cells.[31,32] Although most organisms and eukaryotic cells could not survive in the environment with extreme acidity (pH < 1), there are still some organisms including "acidophilus" and animal organs such as the stomach adapt to such harsh conditions.[33,34] Therefore, maintaining extreme pH homeostasis was also very important. Once the pH was abnormal, it might cause cell dysfunction and serious diseases such as hyperchlorhydria,[35] which was one of the common symptoms of gastrointestinal diseases caused by excessive gastric acid secretion.[36,37] When the pH of gastric juice was less than 1 (normal gastric juice was acidic which the pH was 1.5 to 3.5), the patient would get hyperchlorhydria and suffered from a burning sensation in the stomach, soreness, nausea, and spitting acid.[38] Hyperacidity would damage the stomach and duodenal mucosa, causing diseases such as gastric ulcer or duodenal ulcer.[39,40] Thus, it is highly desirable to develop a gastrointestinal imaging approach with responsibility to the extreme acidic gastric juice environment (pH < 1).

As an FDA (Food and Drug Administration)-approved drug, methylene blue has been used as a NIR contrast agent for the evaluation of the renal function of the animal or the activatable NIR probe by adding a carbamate caging group on the 10-N position.[41−43] In this work, we found that methylene blue could quickly be transformed into NIR-II emissive AIEgens through the protonation of methylene blue in extreme acidic solution. Moreover, the NIR-II emissive AIEgens could be generated in situ in a hyperchlorhydria stomach, which could be used for studying hyperchlorhydria related disease.

Methylene blue (MB) was a typical donor−acceptor (D−A) containing carbonyl-containing heterocycle structures, and we hoped to strengthen the D−A interaction of MB through protonation of a nitrogen-heterocyclic acceptor to result in red-shifted emissions. MB could generate MBH (protonated MB) under acceptor protonation (Figure S1). The absorption peak and emission peak of MBH were red-shifted in comparison with those of MB (Figure 1A,D). Especially, the fluorescence emission peak of MBH was 930 nm, which red-shifted 232 nm (the peak of MB was 698 nm). The MBH shows excellent photostability under 808 nm laser irradiation (Figure S2). Due to the protonated acceptor strengthening the D−A interaction, the fluorescence emission peak can be red-shifted from the NIR-I spectrum range to the NIR-II spectrum range when the protonation occurs in the acceptor of theMB molecule.

Furthermore, the photoluminescence behaviors of MB and MBH in dichloromethane and dichloromethane/*n*-hexane mixtures were investigated. MB showed strong emission in dilute dichloromethane solution and decreased emission with increasing *n*-hexane fraction (f_{Hex}) from 10% to 90%. MB demonstrated a typical aggregation-caused quenching (ACQ) phenomenon, and it was found that MB molecules aggregated into particles in different ratios of *n*-hexane and dichloromethane mixture systems, which caused the decline in MB fluorescence intensity (Figure 1B and C). MBH showed weak fluorescence in dichloromethane solution. The fluorescence of MBH enhanced when the f_{Hex} increased from 10% to 70% but deceased when the f_{Hex} further increased from 80% to 90%. The red line is the DLS measurement results of the MBH molecules aggregated in different *n*-hexane and DCM mixture system ratios. The DLS measurement results showed that a nanoscale aggregate was formed when the ratio of *n*-hexane and DCM mixture systems increased to more than 40%, reaching a hydrodynamic diameter of ∼400 nm when the ratio of *n*-hexane and DCM mixture systems increased to 80%, which was consistent with the trend of the fluorescence measurements (black line in Figure 1F). MBH molecules aggregated into particles in different ratios of *n*-hexane and dichloromethane mixture systems, which led to an increase in MBH fluorescence intensity (Figure 1E and F) and further confirmed the AIE property of MBH. These results displayed achieving ACQ-to-AIE transformation by the protonation of the acceptor in the MB molecule. More importantly, the NIR-II fluorescence emission characteristics and AIE activity after protonation of the molecular receptor of MB generally existed in its analogues, which provide a new strategy for realizing ACQ−AIE conversion (Figure S3).

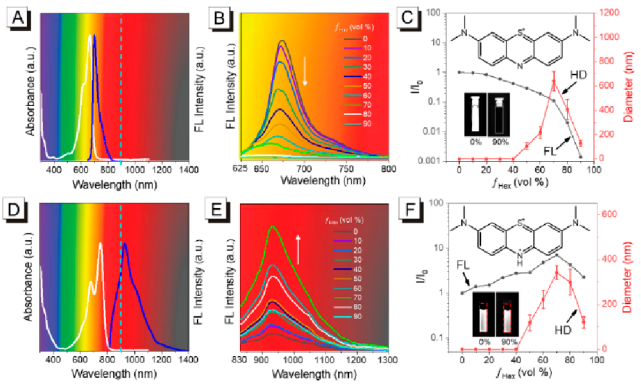

Figure 1. Optical properties of methylene blue (MB) and protonated methylene blue (MBH). (A) UV−vis absorption spectra of MB in aqueous solution. (B) Fluorescence (FL) spectra of MB in hexane/dichloromethane mixtures with different fractions of hexane (f_{Hex}). (C) The curve of the FL intensity and hydrodynamic diameter (HD) of MB versus hexane fractions (f_{Hex}) of hexane/dichloromethane mixtures. (D) UV−vis absorption spectra of MBH in aqueous solution. (E) Fluorescence (FL) spectra of MBH in hexane/dichloromethane mixtures with different fractions of hexane (f_{Hex}). (F) The curve of the FL intensity and hydrodynamic diameter of MBH versus hexane fractions (f_{Hex}) of hexane/dichloromethane mixtures.

As shown in Figure 2, the ^{1}H NMR spectra of MBH indicated the existence of protonation of MB because the proton resonance shift related to the acceptor appeared downfield compared to that of MB. Furthermore, to study

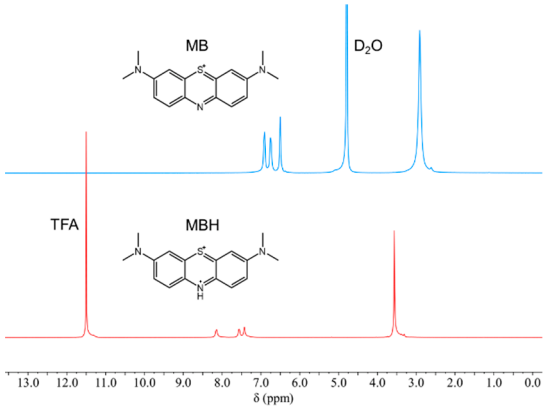

Figure 2. ^{1}H NMR spectra of methylene blue (MB) and protonated methylene blue (MBH).

https://doi.org/10.1021/cbmi.4c00011
Chem. Biomed. Imaging 2024, 2, 683−688

the optical properties of MB to proton (H^+) responses, the standard H^+ titration experiment was carried out. Figure 3A

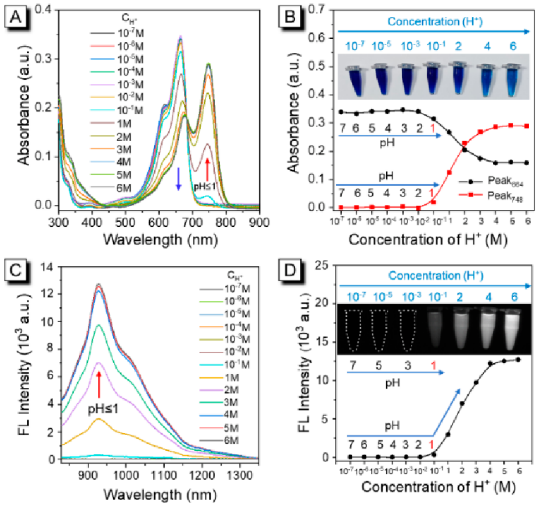

Figure 3. pH responsibility evaluation of methylene blue (MB). (A) UV−vis absorption spectra of MB in different acid solutions. (B) Plot of the absorbance intensity of MB versus acidity. (C) Fluorescence (FL) spectra of MB in different acid solutions. (D) Plot of the FL intensity of MB versus acidity.

and B shows the UV−vis absorption spectral change of MBH at different H^+ concentrations. As the H^+ concentration increased from 10^{-7} to 6 M, the absorbance peak at 664 nm gradually decreased. But from the increase of H^+ concentration from 10^{-1} M (pH 1) to 6 M, a new absorbance peak at 748 nm appeared and slowly rose. Figure 3C demonstrated the NIR-II fluorescence spectral change of MBH at different H^+ concentrations. As the H^+ concentration increased from 10^{-7} to 10^{-2} M (pH 2), the NIR-II fluorescence signal was not detected. However, the H^+ concentration increased from 10^{-1} M (pH 1) to 6 M, a new fluorescence emission in the NIR-II spectrum appeared, and the fluorescence intensity at 930 nm underwent a concomitant monotonic increase. A quantitative analysis of the fluorescence intensity at 930 nm vs H^+ concentration (Figure 3D) revealed the NIR-II fluorescence signal from off to on as the H^+ concentration range was elevated from 10^{-7} M (pH 7) to 6 M. The H^+ concentration of 10^{-1} M (pH 1) was a change point at which the NIR-II fluorescence signal of MBH was from off to on. However, the fluorescence changes of MB relative to H^+ were opposite to those of MBH (Figure S4). Reversible reversibility was another important characteristic for the fluorogenic probe. The pH value of the solution was regulated between 2 and 1 by using hydrochloric acid and aqueous sodium hydroxide. Figure S5 shows that the NIR-II fluorescence signal could be rapidly switched on (pH 1) and off (pH 2) in a reversible manner. The result demonstrated the potential of MB as extreme-acidic-environment activatable NIR-II probes.

Theoretical calculation results showed that electrons were delocalized on the whole molecule backbone (Figure S6). The introduction of acceptor group protons reduced the energy gap (Eg) between the HOMO and LUMO of MBH (1.7935 eV), which was lower than that of MB (2.4797 eV). This was also very consistent with the red-shifted absorption and fluorescence emission spectra in experimental results.

The pH of gastric juice was less than 1, which can cause hyperchlorhydria disease (normal gastric juice was acidic, which the pH was 1.5 to 3.5). There were currently visible and NIR-I fluorescent probes that could be used to detect hypersecretion of gastric acid *in vitro* but not *in vivo*. Compared with the visible and NIR-I imaging, NIR-II fluorescence imaging provided significant improvement of imaging contrast with high spatial resolution. We performed a preliminary experiment to assess a stimuli-responsive MBH probe with activatable NIR-II fluorescence for detecting gastric acid hypersecretion in vivo. Moreover, MB was nontoxic and approved by the FDA. As shown in Figure 4 and Figures S7

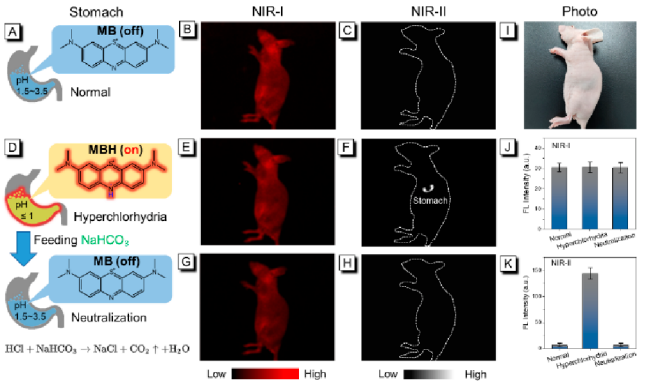

Figure 4. NIR-I imaging versus NIR-II imaging in the mouse stomach. (A) Schematic diagram of mouse stomach imaging in the normal based on the MB probe. (B) NIR-I imaging of mouse stomach in the normal. (C) NIR-II imaging of mouse stomach in the normal. (D) Schematic diagram of mouse stomach imaging in the hyperchlorhydria based on the MBH probe and mouse stomach imaging after neutralization with sodium bicarbonate. (E) NIR-I imaging of mouse stomach in the hyperchlorhydria. (F) NIR-II imaging of mouse stomach in the hyperchlorhydria. (G) After neutralization with sodium bicarbonate, NIR-I imaging of mouse stomach in the hyperchlorhydria. (H) After neutralization with sodium bicarbonate, NIR-II imaging of mouse stomach in the hyperchlorhydria. (I) Mouse photos. (J) NIR-I fluorescence signal of the mouse stomach images as shown in (B), (E), and (G). (K) NIR-II fluorescence signal of the mouse stomach images as shown in (C), (H), and (E).

and S8, when the mouse gastric acid secretion was normal, MB was administered by the gavage method and there was no NIR-II fluorescence signal in the stomach (Figure 4A−C). Subsequently, hydrochloric acid was injected into the stomach of a mouse, which served as an animal model for hypersecretion of gastric acid. The NIR-II fluorescence signal slowly appeared in the stomach (Figure 4D−F). When the mice were given baking soda to neutralize the excess gastric acid, the NIR-II fluorescence signal disappeared (Figure 4H). However, the NIR-I fluorescence signal of the stomach showed almost no change at all and maintained a high background fluorescence signal during the entire operation, because NIR-I images as fluorescence signals had a shorter wavelength and it was largely masked by autofluorescence (Figure 4G). We also monitored the change of the body weight of the mouse after feeding with MB to evaluate their health status; the results showed there was little change for the body weight, indicating the biosafety of MB (Figure S9). Therefore, those results demonstrated that a MBH probe with activatable NIR-II fluorescence provided not only better gastric imaging in vivo

https://doi.org/10.1021/cbmi.4c00011
Chem. Biomed. Imaging 2024, 2, 683−688

but also hyperchlorhydria disease detection accuracy and monitoring of its treatment process.

In summary, we have developed an extreme-acidic-environment detection approach based on the NIR-II fluorogenic process through the protonation of a receptor in MB molecules and successfully applied MB to detect the extremely acidic gastric acid. The protonation of the acceptor in the MB molecule made the fluorescence emission peak red-shift from the NIR-I window to the NIR-II window. More importantly, this was the first example of the realization of the ACQ-to-AIE transformation just through a protonation of an acceptor in a molecule, which provided a unique method for exploring AIE properties in existing materials.

■ ASSOCIATED CONTENT

Supporting Information

The Supporting Information is available free of charge at https://pubs.acs.org/doi/10.1021/cbmi.4c00011.

General informaions, experimental details and supplementary figures S1−S9 (PDF)

Crystallographic Information File for MBH (CIF)

■ AUTHOR INFORMATION

Corresponding Authors

Pengfei Zhang − *Guangdong Key Laboratory of Nanomedicine, CAS-HK Joint Lab of Biomaterials, CAS Key Laboratory of Biomedical Imaging Science and System, Institute of Biomedicine and Biotechnology, Shenzhen Institute of Advanced Technology (SIAT), Chinese Academy of Sciences, Shenzhen 518055, P.R. China;* orcid.org/0000-0003-0390-3806; Email: pf.zhang@siat.ac.cn

Lintao Cai − *Guangdong Key Laboratory of Nanomedicine, CAS-HK Joint Lab of Biomaterials, CAS Key Laboratory of Biomedical Imaging Science and System, Institute of Biomedicine and Biotechnology, Shenzhen Institute of Advanced Technology (SIAT), Chinese Academy of Sciences, Shenzhen 518055, P.R. China; Sino-Euro Center of Biomedicine and Health, Shenzhen 518024, China;* orcid.org/0000-0002-2461-6390; Email: lt.cai@siat.ac.cn

Ben Zhong Tang − *Department of Chemistry, Hong Kong Branch of Chinese National Engineering Research Center for Tissue Restoration and Reconstruction, The Hong Kong University of Science and Technology, Kowloon, Hong Kong 999077, P.R. China; School of Science and Engineering, Shenzhen Institute of Aggregate Science and Technology, The Chinese University of Hong Kong, Shenzhen (CUHK-Shenzhen), Guangdong 518172, P.R. China;* orcid.org/0000-0002-0293-964X; Email: tangbenz@cuhk.edu.cn

Ping Gong − *Guangdong Key Laboratory of Nanomedicine, CAS-HK Joint Lab of Biomaterials, CAS Key Laboratory of Biomedical Imaging Science and System, Institute of Biomedicine and Biotechnology, Shenzhen Institute of Advanced Technology (SIAT), Chinese Academy of Sciences, Shenzhen 518055, P.R. China*; Email: ping.gong@siat.ac.cn

Authors

Guanjun Deng − *Guangdong Key Laboratory of Nanomedicine, CAS-HK Joint Lab of Biomaterials, CAS Key Laboratory of Biomedical Imaging Science and System, Institute of Biomedicine and Biotechnology, Shenzhen Institute of Advanced Technology (SIAT), Chinese Academy of Sciences, Shenzhen 518055, P.R. China*

Siwei Zhang − *Department of Chemistry, Hong Kong Branch of Chinese National Engineering Research Center for Tissue Restoration and Reconstruction, The Hong Kong University of Science and Technology, Kowloon, Hong Kong 999077, P.R. China*

Xinghua Peng − *Guangdong Key Laboratory of Nanomedicine, CAS-HK Joint Lab of Biomaterials, CAS Key Laboratory of Biomedical Imaging Science and System, Institute of Biomedicine and Biotechnology, Shenzhen Institute of Advanced Technology (SIAT), Chinese Academy of Sciences, Shenzhen 518055, P.R. China*

Gongcheng Ma − *Guangdong Key Laboratory of Nanomedicine, CAS-HK Joint Lab of Biomaterials, CAS Key Laboratory of Biomedical Imaging Science and System, Institute of Biomedicine and Biotechnology, Shenzhen Institute of Advanced Technology (SIAT), Chinese Academy of Sciences, Shenzhen 518055, P.R. China*

Luxuan Liu − *Department of Biomedical Engineering, School of Electrical Engineering, University of South China, Hengyang 421002, P.R. China*

Yuyu Tan − *Department of Biomedical Engineering, School of Electrical Engineering, University of South China, Hengyang 421002, P.R. China*

Complete contact information is available at: https://pubs.acs.org/10.1021/cbmi.4c00011

Author Contributions

#G.D., S.Z.: These authors contributed equally.

Notes

The authors declare no competing financial interest.

■ ACKNOWLEDGMENTS

This work was partially supported by National Key R&D Programs (China) (2021YFA0910001, 2023YFA0915400), Guangdong Provincial Key Area R&D Program (2020B1111540001), Shenzhen Basic Research (key project) (China) (JCYJ20210324120011030, JCYJ20210324115804013, and JCYJ20200109114616534), the Shenzhen Science and Technology Program (KQTD20210811090115019), the Major Instrumentation Development Program of the Chinese Academy of Sciences (Project Number: ZDKYYQ20220008), Shenzhen-Macao Technology Plan (SGDX20201103092800301), Technological Cooperation Projects (China) (2020A0505100047), Guangdong Basic and Applied Basic Research Fund Project (China) (2021A1515110699), and Zhuhai Innovation and Entrepreneurship Team Project (ZH011104-05180056PWC). All animal experiments were performed under the protocols approved by the Animal Care and Use Committee (Shenzhen Institutes of Advanced Technology, Chinese Academy of Sciences) (Serial number: SIAT-IACUC-210701-YYS-GP-A1974).

■ REFERENCES

(1) Mo, H. W.; Tsuchiya, Y.; Yan Geng, Y.; Sagawa, T.; Kikuchi, C.; Nakanotani, H.; Ito, F.; Adachi, C. Color tuning of avobenzone boron difluoride as an emitter to achieve full-color emission. *Adv. Funct. Mater.* **2016**, *26*, 6703−6710.

(2) Saito, S.; Nobusue, S.; Tsuzaka, E.; Yuan, C.; Mori, C.; Hara, M.; Seki, T.; Camacho, C.; Irle, S.; Yamaguchi, S. Light-melt adhesive

based on dynamic carbon frameworks in a columnar liquid-crystal phase. *Nat. Commun.* **2016**, *7*, 12094.
(3) Weiss, P. S. 2008 Nobel Prize in Chemistry: green fluorescent protein, its variants and implications. *ACS Nano* **2008**, *2* (10), 1977.
(4) Tian, D.; Qi, F.; Ma, H.; Wang, X.; Pan, Y.; Chen, R.; Zhen Shen, S.; Liu, Z.; Huang, L.; Huang, W. Domino-like multi-emissions across red and near infrared from solid-state 2-/2,6-aryl substituted BODIPY dyes. *Nat. Commun.* **2018**, *9* (1), 2688.
(5) Qin, X.; Liu, X.; Huang, W.; Bettinelli, M.; Liu, X. Lanthanide-activated phosphors based on 4f-5d optical transitions: theoretical and experimental aspects. *Chem. Rev.* **2017**, *117* (5), 4488−4527.
(6) Watson, W. F.; Livingston, R. Concentration quenching of fluorescence in chlorophyll solutions. *Nature* **1948**, *162*, 452−453.
(7) Huang, Y.; Xing, J.; Gong, Q.; Chen, L. C.; Liu, G.; Yao, C.; Wang, Z.; Zhang, H. L.; Chen, Z.; Zhang, Q. Reducing aggregation caused quenching effect through co-assembly of PAH chromophores and molecular barriers. *Nat. Commun.* **2019**, *10*, 169.
(8) Zhang, K.; Liu, J.; Zhang, Y.; Fan, J.; Wang, C.-K.; Lin, L. Theoretical study of the mechanism of aggregation-caused quenching in near-infrared thermally activated delayed fluorescence molecules: hydrogen-bond effect. *J. Phys. Chem. C* **2019**, *123*, 24705−24713.
(9) Wang, J.; Zhao, Y.; Dou, C.; Sun, H.; Xu, P.; Ye, K.; Zhang, J.; Jiang, S.; Li, F.; Wang, Y. Alkyl and dendron substituted quinacridones: synthesis, structures, and luminescent properties. *J. Phys. Chem. B* **2007**, *111*, 5082−5089.
(10) Chen, Y.; Lam, J. W. Y.; Kwok, R. T. K.; Liu, B.; Tang, B. Z. Aggregation-induced emission: fundamental understanding and future developments. *Mater. Horiz.* **2019**, *6*, 428−433.
(11) Hong, Y.; Lam, J. W. Y.; Tang, B. Z. Aggregation-induced emission. *Chem. Soc. Rev.* **2011**, *40*, 5361−5388.
(12) Mei, J.; Leung, N. L.; Kwok, R. T.; Lam, J. W.; Tang, B. Z. Aggregation-induced emission: together we shine, united we soar! *Chem. Rev.* **2015**, *115*, 11718−11940.
(13) Chan, C. Y. K.; Lam, J. W. Y.; Zhao, Z.; Chen, S.; Lu, P.; Sung, H. H. Y.; Kwok, H. S.; Ma, Y.; Williams, I. D.; Tang, B. Z. Aggregation-induced emission, mechanochromism and blue electroluminescence of carbazole and triphenylamine-substituted ethenes. *J. Mater. Chem. C* **2014**, *2*, 4320−4327.
(14) Yang, B.; Niu, X.; Huang, Z.; Zhao, C.; Liu, Y.; Ma, C. A novel kind of dimmer (excimer)-induced-AIE compound 2-phenylisothiazolo[5,4-b] pyridin-3(2H)-one as high selective bisulfite anion probe. *Tetrahedron* **2013**, *69*, 8250−8254.
(15) Shih, P. I.; Chuang, C. Y.; Chien, C. H.; Diau, E. W. G.; Shu, C. F. Highly efficient non-doped blue-light-emitting diodes based on an anthrancene derivative end-capped with tetraphenylethylene groups. *Adv. Funct. Mater.* **2007**, *17*, 3141−3146.
(16) Park, S. H.; Kwon, N.; Lee, J. H.; Yoon, J.; Shin, I. Synthetic ratiometric fluorescent probes for detection of ions. *Chem. Soc. Rev.* **2020**, *49*, 143−179.
(17) Li, C.; Chen, G.; Zhang, Y.; Wu, F.; Wang, Q. Advanced fluorescence imaging technology in the near-infrared-II window for biomedical applications. *J. Am. Chem. Soc.* **2020**, *142*, 14789−14804.
(18) Yuan, L.; Lin, W.; Zheng, K.; He, L.; Huang, W. Far-red to near infrared analyte-responsive fluorescent probes based on organic fluorophore platforms for fluorescence imaging. *Chem. Soc. Rev.* **2013**, *42*, 622−61.
(19) Hong, G.; Antaris, A. L.; Dai, H. Near-infrared fluorophores for biomedical imaging. *Nat. Biomed. Eng.* **2017**, *1*, 0010.
(20) Deng, G.; Peng, X.; Sun, Z.; Zheng, W.; Yu, J.; Du, L.; Chen, H.; Gong, P.; Zhang, P.; Cai, L.; Tang, B. Z. Natural-killer-cell-inspired nanorobots with aggregation-induced emission characteristics for near-infrared-II fluorescence-guided glioma theranostics. *ACS Nano* **2020**, *14*, 11452−11462.
(21) Deng, G.; Cheung, F. M. H.; Sun, Z.; Peng, X.; Li, S.; Gong, P.; Cai, L. Near-infrared fluorescence imaging for vascular visualization and fungal detection in plants. *Chem. Commun.* **2018**, *54*, 13240−13243.
(22) Hong, G.; Diao, S.; Chang, J.; Antaris, A. L.; Chen, C.; Zhang, B.; Zhao, S.; Atochin, D. N.; Huang, P. L.; Andreasson, K. I.; Kuo, C. J.; Dai, H. Through-skull fluorescence imaging of the brain in a new near-infrared window. *Nat. Photonics* **2014**, *8*, 723−730.
(23) Li, B.; Zhao, M.; Feng, L.; Dou, C.; Ding, S.; Zhou, G.; Lu, L.; Zhang, H.; Chen, F.; Li, X.; Li, G.; Zhao, S.; Jiang, C.; Wang, Y.; Zhao, D.; Cheng, Y.; Zhang, F. Organic NIR-II molecule with long blood half-life for in vivo dynamic vascular imaging. *Nat. Commun.* **2020**, *11*, 3102.
(24) Li, Y.; Cai, Z.; Liu, S.; Zhang, H.; Wong, S. T. H.; Lam, J. W. Y.; Kwok, R. T. K.; Qian, J.; Tang, B. Z. Design of AIEgens for near-infrared IIb imaging through structural modulation at molecular and morphological levels. *Nat. Commun.* **2020**, *11*, 1255.
(25) Li, C.; Li, W.; Liu, H.; Zhang, Y.; Chen, G.; Li, Z.; Wang, Q. An activatable NIR-II nanoprobe for in vivo early real-time diagnosis of traumatic brain injury. *Angew. Chem., Int. Ed.* **2020**, *59*, 247−252.
(26) Zhu, T.; Ren, N.; Liu, X.; Dong, Y.; Wang, R.; Gao, J.; Sun, J.; Zhu, Y.; Wang, L.; Fan, C.; Tian, H.; Li, J.; Zhao, C. Probing the intracellular dynamics of nitric oxide and hydrogen sulfide using an activatable NIR II fluorescence reporter. *Angew. Chem., Int. Ed.* **2021**, *60*, 8450−8454.
(27) Ling, S.; Yang, X.; Li, C.; Zhang, Y.; Yang, H.; Chen, G.; Wang, Q. Tumor microenvironment-activated NIR-II nanotheranostic system for precise diagnosis and treatment of peritoneal metastasis. *Angew. Chem., Int. Ed.* **2020**, *59*, 7219−7223.
(28) Yang, Z.; Cao, J.; He, Y.; Yang, J. H.; Kim, T.; Peng, X.; Kim, J. S. Macro-/micro-environment-sensitive chemosensing and biological imaging. *Chem. Soc. Rev.* **2014**, *43*, 4563−4601.
(29) Xu, L.; Fidler, J. I. Acidic pH-induced elevation in interleukin 8 expression by human ovarian carcinoma cells. *Cancer Res.* **2000**, *60*, 4610−4616.
(30) Demaurex, N. pH homeostasis of cellular organelles. *Physiology* **2002**, *17*, 1−5.
(31) Aoi, W.; Marunaka, Y. Importance of pH homeostasis in metabolic health and diseases: crucial role of membrane proton transport. *BioMed. Res. Int.* **2014**, *2014*, 1−8.
(32) Baker-Austin, C.; Dopson, M. Life in acid: pH homeostasis in acidophiles. *Trends Microbiol.* **2007**, *15* (4), 165−171.
(33) Ma, G.; Gao, X.; Jiang, C.; Xing, S.; Wei, C.; Huang, P.; Lin, J. pH-responsive nanoprobe for in vivo photoacoustic imaging of gastric acid. *Anal. Chem.* **2019**, *91*, 13570−13575.
(34) Yoon, J.; Joseph, J.; Waterhouse, D. J.; Luthman, A. S.; Gordon, G. S. D.; di Pietro, M.; Januszewicz, W.; Fitzgerald, R. C.; Bohndiek, S. E. A clinically translatable hyperspectral endoscopy (HySE) system for imaging the gastrointestinal tract. *Nat. Commun.* **2019**, *10* (1), 1902.
(35) Yang, M.; Song, Y.; Zhang, M.; Lin, S.; Hao, Z.; Liang, Y.; Zhang, D.; Chen, P. R. Converting a solvatochromic fluorophore into a protein-based pH indicator for extreme acidity. *Angew. Chem., Int. Ed.* **2012**, *51*, 7674−7679.
(36) Turck, F. B. Hyperchlorhydria. *Med. Rec.* **1910**, *77*, 261.
(37) Lu, P. J.; Hsu, P. I.; Chen, C. H.; Hsiao, M.; Chang, W. C.; Tseng, H. H.; Lin, K. H.; Chuah, S. K.; Chen, H. C. Gastric juice acidity in upper gastrointestinal diseases. *World J. Gastroenterol.* **2010**, *16*, 5496−5501.
(38) Walsh, J. H.; Richardson, C. T.; Fordtran, J. S. pH dependence of acid secretion and gastrin release in normal and ulcer subjects. *J. Clin. Invest.* **1975**, *55* (3), 462−468.
(39) Rolph, F. W. Gastric hyperacidity. *Can. Med. Assoc. J.* **1914**, *4*, 25−32.
(40) Martinsen, T. C.; Fossmark, R.; Waldum, H. L. The phylogeny and biological function of gastric juice—microbiological consequences of removing gastric acid. *Int. J. Mol. Sci.* **2019**, *20*, 6031.
(41) Xue, D.; Wu, Di.; Lu, Z.; Neuhaus, J.; Zebibula, A.; Feng, Z.; Cheng, S.; Zhou, J.; Qian, J.; Li, G. Structural and Functional NIR-II Fluorescence Bioimaging in Urinary System via Clinically Approved Dye Methylene Blue. *Engineering* **2023**, *22*, 149−158.
(42) Li, S.; Wang, P.; Yang, K.; Liu, Y.; Cheng, D.; He, L. Methylene blue-based near-infrared activatable probes for bioimaging. *Dyes. Pigm.* **2023**, *211*, 111083.

https://doi.org/10.1021/cbmi.4c00011
Chem. Biomed. Imaging 2024, 2, 683−688

(43) Ma, G.; Dirak, M.; Liu, Z.; Jiang, D.; Wang, Y.; Xiang, C.; Zhang, Y.; Luo, Y.; Gong, P.; Cai, L.; Kolemen, S.; Zhang, P. Rechargeable Afterglow Nanotorches for In Vivo Tracing of Cell-Based Microrobots. *Angew. Chem., Int. Ed.* **2024**, No. e202400658.

https://doi.org/10.1021/cbmi.4c00011
Chem. Biomed. Imaging 2024, 2, 683−688